Earth Systems, Resources, and Sustainability, 2026, 1(3), 249–264

Scilight

Earth Systems, Resources, and Sustainability

Journal Homepage: https://www.sciltp.com/journals/esrs

Article

Geochemical Signature of PGE Mineralization in the Torappadi Ultramafic–Mafic Complex, Southern India

S. Velladurai [1,2,*], V. Kumaravel [2,*], J. Prabhakar [3], S.S. Chinnasamy [4], P. Devarajan [1] and Yogendra Bhogta [5]

[1] Geological Survey of India, State Unit: Tamil Nadu and Puducherry, Chennai 600032, India
[2] Department of Geology, Central University of Tamil Nadu, Thiruvarur 610005, India
[3] Geological Survey of India, North-Eastern Region, Shillong 793006, India
[4] Department of Earth Sciences, Indian Institute of Technology Bombay, Powai, Mumbai 400076, India
[5] Geological Survey of India, State Unit: Jharkhand, Ranchi 834004, India
[*] Correspondence: svdurai86@gmail.com (S.V.); vkumaravel@gmail.com (V.K.)

ABSTRACT

The Torappadi Ultramafic–Mafic Complex (TUC) in the Southern Granulite Terrain (SGT) is mainly composed of pyroxenite (websterite) and gabbro along with their variants—orthopyroxenite, diopsidite, gabbroic anorthosite and anorthositic gabbro was investigated for PGE mineralization. Orthopyroxene (enstatite), clinopyroxene (chrome diopside), plagioclase feldspar ($An_{57–73\%}$) and primary hornblende (magnesio-hornblende) are the major minerals largely present in TUC in the order of decreasing abundance. The MgO values in enstatite rich pyroxenite ranges between 17.15–30.78 wt%, it varies from 25.21 to 32.19 wt% for chrome diopside rich pyroxenite while the MgO wt% in gabbro ranges between 10.5 and 25.5. A total of 145 rock samples from pyroxenite (81), ortho-pyroxenite (13), diopsidite (7) and gabbro (44) were analysed for Platinum Group Elements (PGE). The total PGE (ΣPGE) in the pyroxenite ($N = 94$) varies from 16.2 to 380.5 ppb, it ranges between 14.1 ppb and 117.4 ppb in gabbro ($N = 44$) while the diopsidite ($N = 7$) analyzed from 54.7 to 272.7 ppb. The PGE mineralization in TUC appears to be lithologically controlled. However, the elevated ΣPGE content around fold hinges (F_1 and F_2) provides evidence limited re-distribution of PGE during deformational event. Wide range of ΣREE (8–1021 ppm), LaN/SmN (0.58–6.10), and GdN/YbN (0.08–6.69) ratios, indicate significant post magmatic deformation assisted fluid–rock interaction. The primitive mantle-normalized Ni–Cu–PGE patterns of the pyroxenites and gabbro of TUC indicate that these rocks were formed from an evolved mafic magma that experienced early silicate fractionation and sulfide saturation. The ratios of Pd vs. Cu/Pd, and Cu vs. Pd, suggest that the TUC sequence might have been evolved through mantle derived, episodic magmatic pulses with early-stage sulphur fractionation.

ARTICLE INFO

History:

Received 19 November 2025
Revised 4 March 2026
Accepted 11 March 2026
Published: 17 March 2026

Keywords:

Torappadi Ultramafic–Mafic Complex;
PGE mineralization;
pyroxenite and gabbro

Citation:

Velladurai, S.; Kumaravel, V.; Prabhakar, J.; et al. Geochemical Signature of PGE Mineralization in the Torappadi Ultramafic–Mafic Complex, Southern India. *Earth Systems, Resources, and Sustainability* **2026**, *1*(3), 249–264. https://doi.org/10.53941/esrs.2026.100015

Copyright: © 2026 by the authors. This is an open access article under the terms and conditions of the Creative Commons Attribution (CC BY) license (https://creativecommons.org/licenses/by/4.0/).
Publisher's Note: Scilight stays neutral with regard to jurisdictional claims in published maps and institutional affiliations.

Research Highlights

- PGE distribution in Torappadi Ultramafic–Mafic Complex is controlled by both the structure as well as lithology.
- The total PGE (ΣPGE) in the Ultramafic–Mafic rocks of Torappadi Complex varies from 14.1 to 380.5 ppb.
- The PGE and trace element geochemistry indicates that the TUC evolved through episodic magmatic pulses.

1. Introduction

The Platinum Group Elements (PGEs) comprising platinum (Pt), palladium (Pd), rhodium (Rh), ruthenium (Ru), iridium (Ir), and osmium (Os) are classified as critical and strategic metals due to their extensive industrial applications in catalysts, electronics and emerging green energy technologies [1, 2]. They have similar physical and chemical properties and tend to occur together in the same mineral deposits. Most important ores of PGE are as follows: Erlichmanite and laurite (sulphides), irarsite, osarsite, sperrylite (arsenides), anduoite, gersdoffite, osmiite, rutheniridosmine and ruarsite [3–5]. Based on their geochemical behaviour, PGEs are subdivided into two groups: the compatible Ir-group PGEs (IPGEs: Os, Ir and Ru) and the incompatible Pt-group PGEs (PPGEs: Rh, Pd and Pt) [6, 7]. These elements are typically associated with mafic–ultramafic complexes and layered intrusions formed through magmatic differentiation and sulfide segregation processes [6, 8–10].

The PGE mineralization is commonly associated with magmatic Ni–Cu deposits, either as by-product or as massive deposit [2, 11, 12]. Ultramafic–mafic magma emplacement in different tectonic environments is the major favourable loci for PGE and associated metal distribution and enrichments [2, 13]. PGEs exhibit strong siderophile and chalcophile affinities [14–16] and serve as sensitive indicators of magmatic processes such as partial melting, crystal fractionation and sulfur saturation [6, 14, 17]. Orthomagmatic processes are known to scavenge PGEs and other chalcophile elements (e.g., Au, Ag, As, Cd, Bi, Ni, Co, Pb, Re, Sb, Te and Zn), leading to the formation of Cu–Ni sulfides, chromite and PGE-bearing ore deposits [18–22]. Ni and PGE deposits occur in intra-continental rift settings (e.g., Norilsk, Russia [2]) as well as in convergent settings (Aguablanca, Spain [23]); tholeiitic intrusion (Pechenga, Russia [24]) and komatiiitic flows/intrusion (Kambalda, Australia [25]); primary magmatic concentrations (Duluth, USA [2]) and late magmatic enrichments (Merensky reef, South Africa [26]). Therefore, the distribution and geochemical characteristics of PGEs provide valuable insights into ore-forming mechanisms and play a key role in understanding the nature and tectonic settings of parental magma and thus evaluating the mineral resource potential of mafic–ultramafic complexes.

In India, PGE occurrences have been reported from several ultramafic–mafic complexes of Precambrian terranes, notably the Sukinda and Baula–Nuasahi Complexes (Odisha) [27, 28], Gondpipri mafic–ultramafic layered Intrusion (Maharashtra) [29], Madawara Igneous Complex, (Uttar Pradesh) [30], the Hanumalapur Complex (Karnataka) [31], and the Sittampundi Anorthosite Complex (Tamil Nadu) [32, 33]. The total resource of Platinum Group of Metals (PGM) in India is estimated to be 15 tonnes (UNFC system), concentrated at Nilgiri, Boula-Nuasahi and Sukinda in Orissa [33]. About 54% of this is in 'pre-feasibility' category and the remaining under 'inferred' category [33, 34]. Besides quantifiable PGE deposits, there are several incidence and occurrences of PGE mineralization associated with ultramafic–mafic complexes is reported in Shillong Plateau, Singhbhum Craton, Bundelkhand Craton, Bastar Craton and elsewhere in India [27, 35–39]. Similarly, there are several ultramafic–mafic complexes reported in Tamil Nadu viz., Sittampundi Anorthosite Complex (SAC), Mettupalaiyam Ultramafic Complex (MUC), Samalapatti, Torappadi, Kadavur, Oddanchattiram and Arumanallur complexes. However, the Sittampundi and Mettupalaiyam Complexes represent Archean layered sequences of pyroxenites, chromitite, garnet-pyroxene granulite, gabbro, gabbroic anorthosite and anorthosite are well studied in the aspects of PGE distribution and their resource potential [31, 33, 40] while, other ultramafic–mafic complexes in Tamil Nadu gained limited attention.

The Torappadi Ultramafic–Mafic Complex (TUC), one of the ultramafic–mafic complexes of Tamil Nadu located within the Archean crustal domain of Southern Granulite Terrain, provide a favorable geological setting for investigating magmatic processes and associated PGE mineralization (Figure 1) [41]. Although the presence of ultramafic rocks in the Torappadi area has been recognized for several decades, earlier studies primarily emphasized petrographic descriptions of the Torappadi Ultramafic–Mafic Complex [42–44] and their potential on the PGE mineralization yet to be attempted.

Therefore, the present study aims to evaluate the PGE geochemistry and mineralization characteristics of the Torappadi Ultramafic–Mafic Complex, Tiruvannamalai District, Tamil Nadu (Figures 1 and 2). Geochemical analyses, integrated with petrographic and mineralogical observations, are employed to elucidate the processes governing PGE enrichment and to assess the economic potential of the studied rocks. This work contributes to the broader understanding of nature of parental magma characteristics, deformation and PGE distribution in Torappadi area and also provides essential baseline data and scope for future mineral exploration strategies in the region.

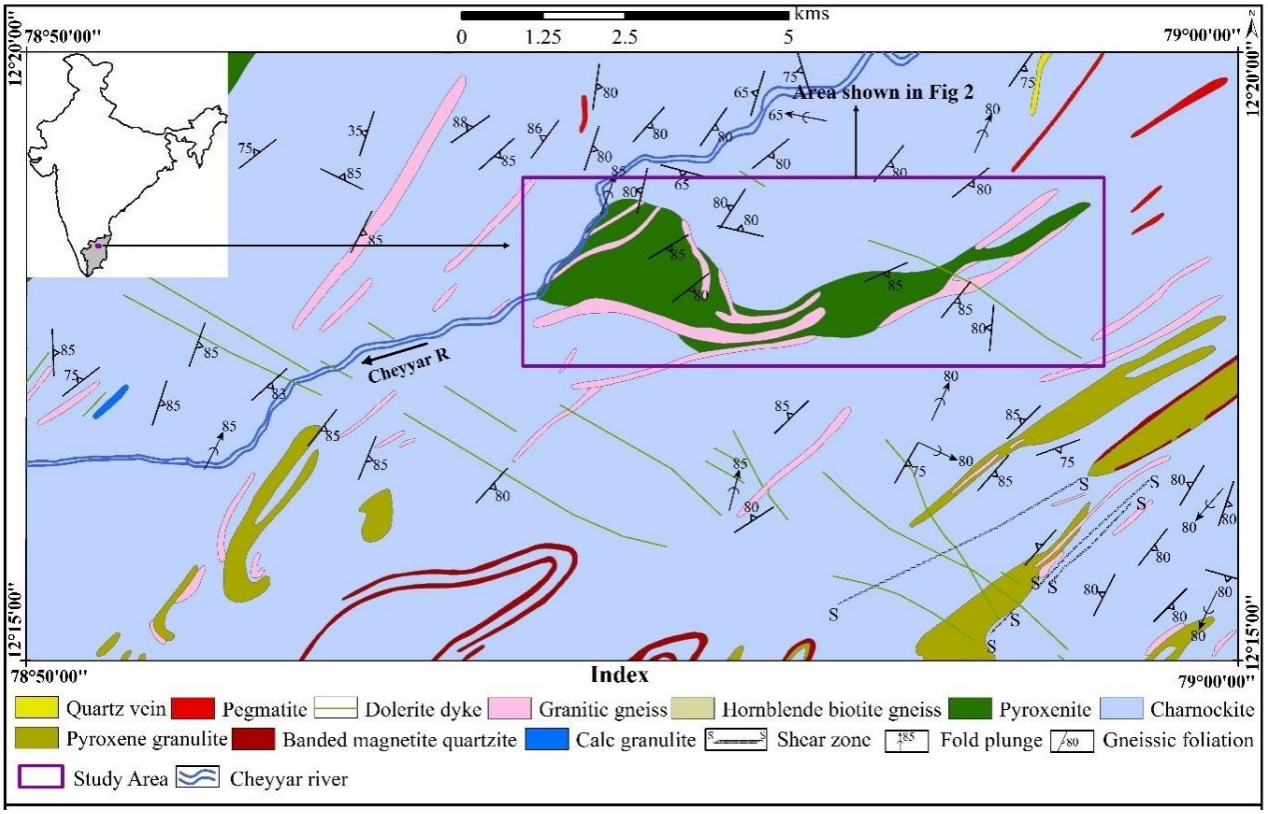

Figure 1. Location of Torappadi Ultramafic–Mafic Complex (TUC), Tamil Nadu, India in the regional geological map (Modified after [45, 46]).

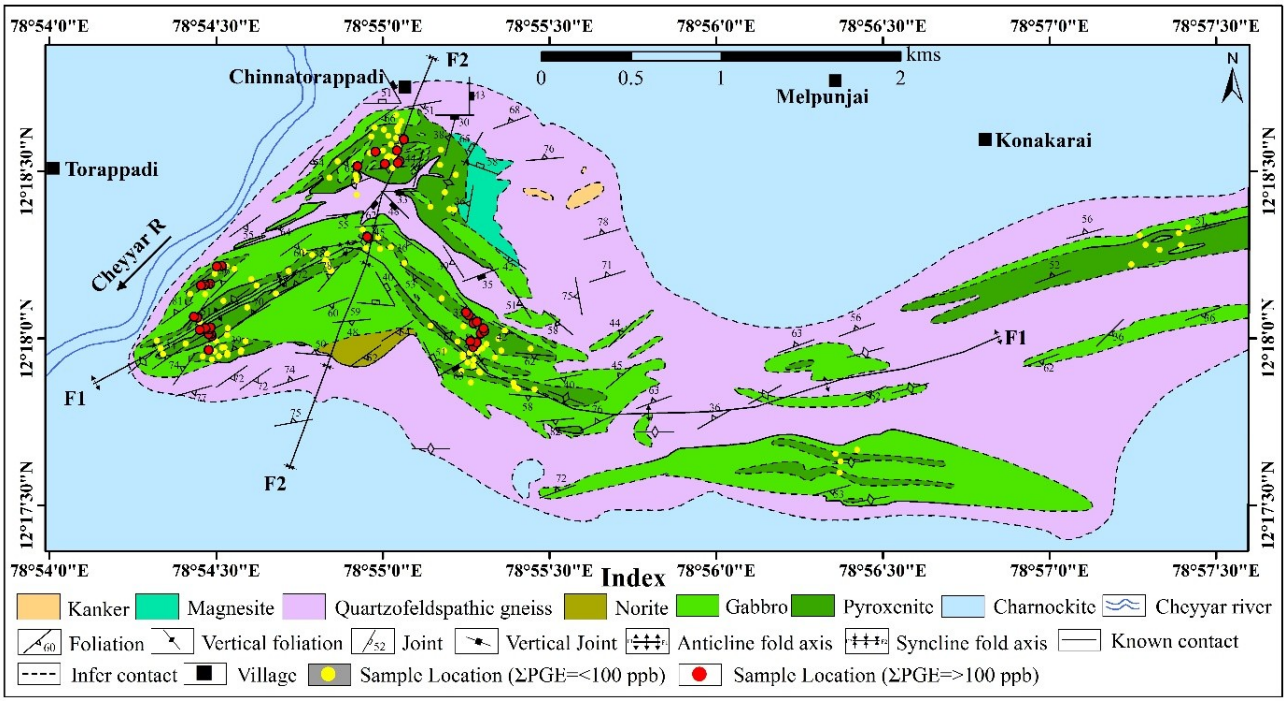

Figure 2. Geological map of Torappadi Ultramafic–Mafic Complex (TUC) with lithological assemblages and their contact relationship, major structural features and sample locations (Modified after [47]).

2. Geology of the Torappadi Ultramafic–Mafic Complex (TUC)

TUC is located in the western part of the Madras Block and regionally the area is composed of pyroxene granulite, charnockite, garnetiferous biotite gneiss, granite gneiss, pink granite, and younger intrusives (pegmatite, quartz veins, and dolerite dykes) [43, 44]. The general strike of foliation/banding of the area ranges from NNE-SSW to NE-SW with local variations in NW-SE and E-W directions, with converging and opposing dips ranging from 45° and more to vertical indicating the progressive deformation. Most of the rocks in the area show shearing effects such as slickenside, trapshooting, mylonitization, formation of epidote and chert veins.

The area around TUC is mainly characterized by Charnockite Group of rocks charnockite, pyroxene granulite and banded magnetite quartzite (BMQ)] and quartzofeldspathic gneiss by migmatised charnockite and pink gneissic granite inter banded with dominant in the area occupying both hills and plains, It is bluish grey to dark in colour with brownish tint on the weathered surface, medium to coarse grained and on fresh surface greasy in appearance and composed of quartz, feldspar, biotite, pyroxene and garnet at places. Charnockite is found to be occurring as xenoliths within quartzofeldspathic gneiss and spatially associated with banded magnetite quartzite and pyroxene granulite. The pyroxene granulite is a dark, coarse grained, granular texture and consists of pyroxene, feldspar, quartz and hornblende as major minerals and biotite and magnetite as accessary minerals. It occurs as concordant lenses in charnockite, and petrographic study reveals that the hypersthene is predominant over augite.

The TUC is represented by positive topography, generally called Torappadi hill, with pyroxenite, gabbro and their respective variants (orthopyroxenite, diopsidite, gabbroic anorthosite and anorthositic gabbro) (Figure 3) that forms an arcuate band swerving about NE-SW to ENE-WSW direction and the convex side of the body pointing towards north. The grain size and mineralogy variations are observed both along the strike as well as along the dip direction. Pyroxenite occurs as detached and discontinuous bands in association with gabbro, gabbroic anorthosite and anorthositic gabbro in Torappadi hill and has sharp contact with associated rocks (Figure 3D,E). At places, the pyroxenite shows cumulus texture (Figure 3A). The bands mostly trend in NE-SW and NW-SE direction. Total eleven major pyroxenite bands have been demarcated in the Torappadi hill and its surrounding area. The width of these bands varies from 60 to 300 m and length varies from 0.4 to 1.3 km. Mineralogically, it is dominated by orthopyroxene (enstatite), followed by clinopyroxene (chrome diopside), primary hornblende (magnesio-hornblende) and plagioclase feldspar ($An_{57–73\%}$) as major mineral. The proportion of both enstatite and chrome diopside in pyroxenite [websterite: both clino and ortho pyroxene in significant amount (>10%)] vary from place to place. Major portion of the pyroxenite in this complex is composed of websterite (enstatite and chrome diopside). The rock shows monomineralic in nature at places in smaller scale, based on which it has been classified as ortho-pyroxenite (>90% Enstatite) and diopsidite (>90% diopside) (Figure 3B,C). The diopsidite and ortho-pyroxenite occur as thin bands and lenses within the pyroxenite (websterite). Gabbro forms the major mafic rocks of the area (Figure 4A,B). Plagioclase content varies from place to place and with the increase and decrease of plagioclase, the rock becomes gabbroic anorthosite to anorthositic gabbro (Figure 4C,D). Under the microscope, the rock exhibits granulitic texture, medium to coarse grained and composed of enstatite ($En_{59–60\%}$), plagioclase feldspar ($An_{57–60\%}$) and chrome diopside.

Three phases of deformation were recognized in the region through a detailed structural analysis [48]. The first generation (F_1) fold is upright, tight isoclinals in nature with steep dipping axial plane varying from E-W to NE-SW trend. The NE-SW trending second generation fold (F_2) developed on a regional scale as a long canoe shaped tight isoclinals folds resulting in a series of antiforms and synforms. The F_3 fold is identified as broad wraps along WNW-ESE to NW-SE direction. The pyroxene granulite and banded magnetite quartzite bands serve as marker horizons to decipher the fold pattern in the region.

Two generations of folding (F_1 and F_2) were mapped which are complementary with the regional structure. The earlier fold (F_1) is a tight isoclinal fold, the axial trace of which trends in a NE-SW direction. This fold is clearly seen as a mappable scale fold in the southwestern slope of the Torappadi hill. Both the limbs are refolded along NNE-SSW direction (F_2). This second fold is an open asymmetrical fold and the axial trace of the fold runs along the axial region of Torappadi ridge. Minor warping along NNE-SSW directions is also seen, which appears to be the sympathetic folds parallel to F_2 fold. The axial traces of the major folds (F_2) trends along N10° to 55° E–S10° to 55° W, which influenced the course of the Cheyyar River along this later deformation trend.

Despite this polyphase deformation history, PGE mineralization in the complex appears to be dominantly controlled by lithology governed by the magmatic processes during initial stage of emplacement however, the occurrence of PGE phases along fractures indicate that localized redistribution of PGE did occur, most likely during D_1 and D_2 deformation, facilitated by micro-fracturing and limited fluid ingress. The sample location and distribution of PGE in TUC is shown in Figure 2 and further discussion is followed in the subsequent sections.

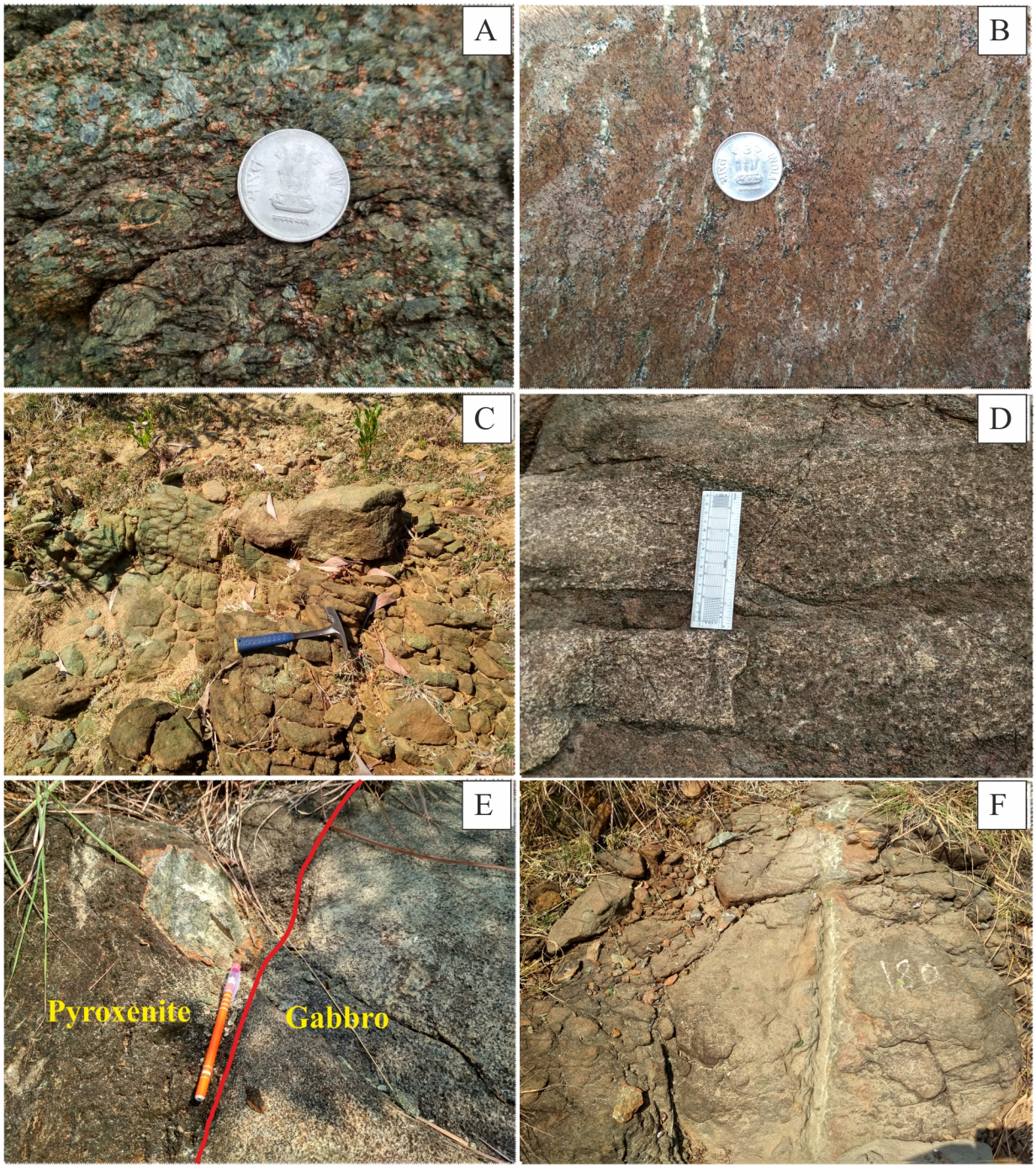

Figure 3. Field photographs of pyroxenite in Torappadi Ultramafic–Mafic Complex. (**A**) Showing cumulus texture in pyroxenite; (**B**) Orthopyroxenite with thin magnesite veins; (**C**) Diopsidite occurrence in Torappadi Hill; (**D**) Disposition of thin pyroxenite layers within gabbro; (**E**) Showing a sharp contact between pyroxenite and gabbro; (**F**) Showing channel sampling in pyroxenite.

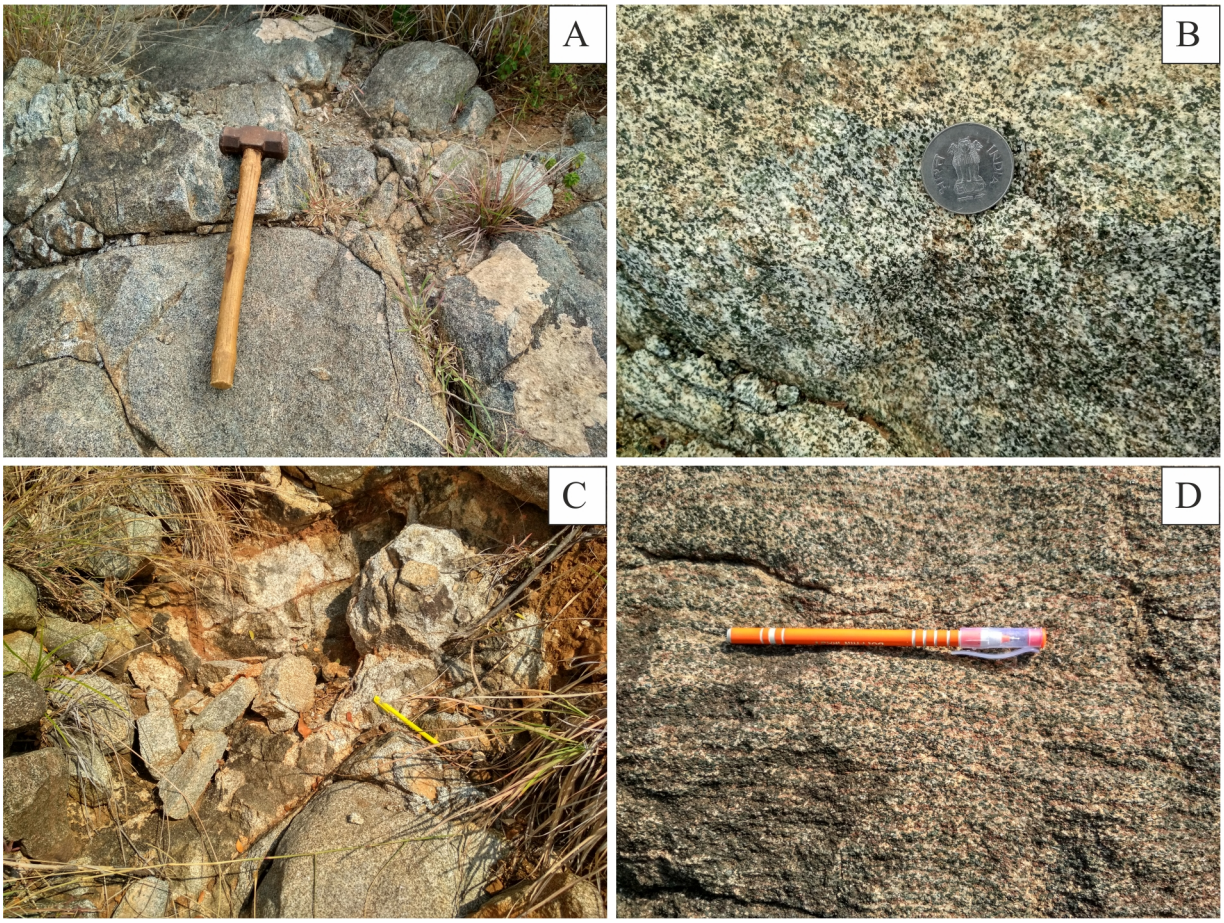

Figure 4. Field photographs of gabbro and its variants in Torappadi Ultramafic–Mafic Complex; (**A**) Occurrence of gabbro in Torappadi hill; (**B**) Close view of gabbro; (**C**) Gabbroic anorthosite; (**D**) Anorthositic gabbro.

3. Methodology

A total of 20 samples were collected from representative lithologies of Ultramafic–Mafic rocks to study petrochemical nature. 14 samples were collected from pyroxenite (websterite), which include three types based on the mineralogical proportion of enstatite and chrome diopside; (a) enstatite rich pyroxenite [enstatite $>$ chrome diopside (10 nos.)], (b) chrome diopside rich pyroxenite [chrome diopside $>$ enstatite (2 nos.)], (c) equal proportion of both varieties [enstatite $\leq$ chrome diopside (2 nos.)], one sample from diopsidite and five samples were collected from gabbroic rocks like gabbro (4 nos.) and anorthositic gabbro (1 no). In addition, a total of 145 bed rock samples (BRS) were collected by channel chip method (Figure 3F), from pyroxenite (81), ortho-pyroxenite (13), diopsidite (7) and gabbro (44). In which, 128 samples were collected in three profiles, in pyroxenite bands samples have been collected at 10 m interval along profile whereas, 20 to 25 m sample interval has been followed in the mafic portion. In both cases, each sampling channel was maintained for 1.0 m length. These samples were powdered to -200 mesh for trace element and PGE analysis.

The major oxides and minor elements were analyzed by X-ray Fluorescence Spectroscopy (XRF) and Rare Earth Elements, PGE and trace elements were analyzed by Inductively Coupled Plasma-Mass Spectroscopy (ICP-MS), at the GSI Lab, SR, Hyderabad following the standard operation procedure. A total of 15 samples from TUC were studied under SEM-EDS and EPMA to assess the mineral-chemical characters of the constituent phases at GSI, SR, Hyderabad.

4. Results

4.1. Petrochemistry

The MgO values in enstatite rich pyroxenite ranges between 17.15–30.78 wt%, it varies from 25.21 to 32.19 wt% for chrome diopside rich pyroxenite and for gabbro it ranges between 10.5 and 25.5 wt% and the Mg# are 84.2–90%, 90–91.3%, 81.4–87.2%, respectively. The high Mg# indicates the primitive nature and differentiation of Torappadi Ultramafic–Mafic Complex. Overall, the TiO_2 content is restricted to 0.07–0.33 wt% (Supplementary Table S1). The compatible trace elements Ni and Cr in pyroxenite (enstatite rich, chrome diopside rich and equal proportion of both varieties) ranges from 500 to 1071 ppm and from 1969 to 7273 ppm, respectively. The abundance of Ni and Cr in pyroxenite shows broad positive correlation when plotted against Mg# (Figure 5). The positive relation

of compatible trace elements with Mg# and their elevated abundance indicate the primary magmatic signatures. A Jenson cation plot [49] showing that the MgO-rich pyroxenite, diopsidite and gabbro fall in a tight group within Komatiitic field (Figure 6).

The trace element and PGE distribution in Pyroxenite (websterite):

4.1.1. Enstatite Rich Pyroxenite

A total of 60 samples were collected from enstatite rich pyroxenite, in which the Cu range between 5 to 605 ppm, average of 54 ppm, Co between 52 to 120 ppm, average of 77 ppm, Ni varies from 268 to 1044 with average 608 ppm and Cr vary from 400 to 6400 ppm, average of 3614 ppm. The Pt + Pd shows a value from 7 to 344 ppb, average of 81 ppb. The highest Pt + Pd value (344 ppb) is recorded in sample TW-41, collected from the isolated northern band. The elements Ir, Ru and Rh are not shown any significant values. In ortho-pyroxenite, 13 samples were collected, here the Cu is ranges between 14 to 285 ppm, with an average of 84 ppm, Co varies from 52 to 106 ppm, average of 77 ppm, Ni range from 240 to 670 ppm, average of 528 ppm, Cr is between 500 to 5000 ppm. The Pt + Pd show a value range between 15 to 115 ppb, average of 51 ppb. The elements Ir, Ru and Rh are not shown any significant value. From gabbroic rocks (occur as hanging wall and foot wall), 40 samples have been collected. The distribution of Cu ranges from 1.5 to 295 ppm, average of 50 ppm, Co vary from 45 to 96 ppm, average of 72 ppm, Ni is between 155 to 860 ppm, average of 495 ppm and the Cr is range from 300 to 8500 ppm, average of 2972 ppm. The total Pt + pd values vary from 9 to 106 ppb, average of 44 ppb.

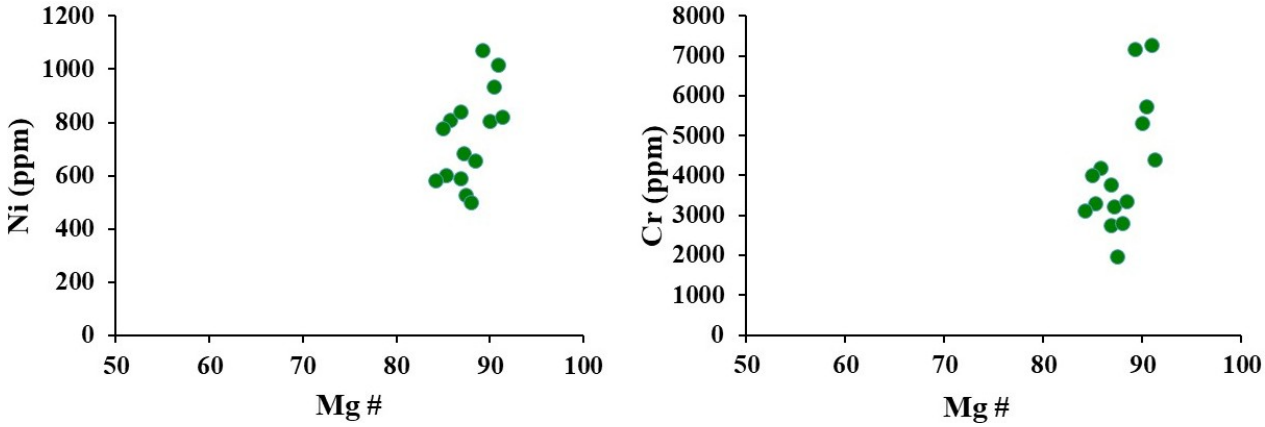

Figure 5. Compatible trace elements (Ni and Cr) vs. Mg# variation plots for pyroxenites of TUC reflect the parental magma nature.

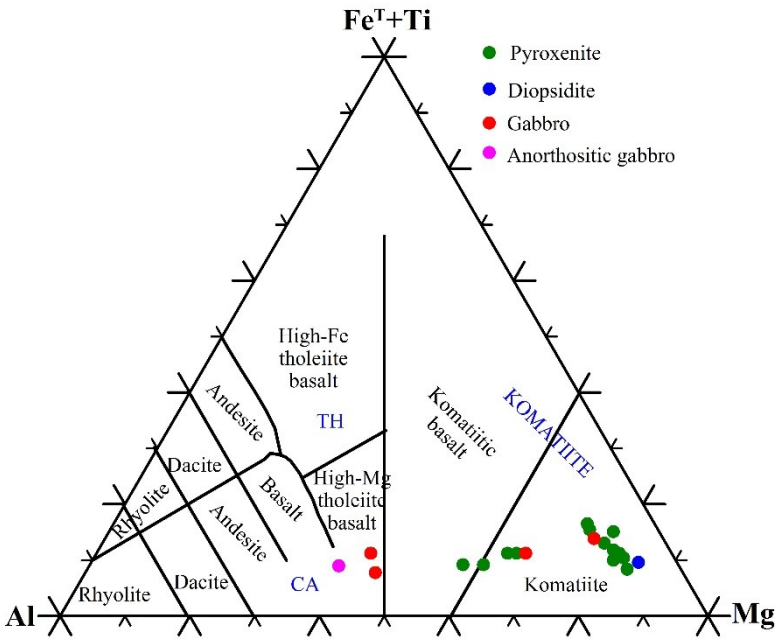

Figure 6. Jensen cation plot [49] of pyroxenite, diopsidite, gabbro and anorthositic gabbro from Torappadi Ultramafic–Mafic Complex cluster in komatiite field.

4.1.2. Chrome Diopside Rich Pyroxenite

From chrome diopside rich pyroxenite, 13 samples were collected, in which Cu ranges between 5 to 111 ppm, average of 29 ppm, Co between 65 to 97 ppm, average of 78 ppm, Ni vary from 411 to 1090 with average of 674 ppm and Cr varies from 1300 to 5400 ppm, average of 3800 ppm. The Pt + Pd shows a value from 12 to 248 ppb, average of 68 ppb. In diopsidite (diopside rich), seven samples have been collected, in which the Cu values range between 8 to 21 ppm, average 14 ppm, Co range from 61 to 80 ppm, average 71 ppm, Ni vary from 444 to 619 ppm, average 519 ppm, Cr is between 4100 to 6000 ppm, average 4937 ppm. The total Pd + Pt values from 39 to 145 ppb, average 76 ppb. The gabbro (4 nos.) samples, show that the value of Cu 26 ppm, Co 73 ppm, Ni 440 ppm, Cr 3100 ppm, and Pt + Pd 96 ppb. The elements Ir, Ru and Rh is not shown any significant value.

4.1.3. Pyroxenite with Equal Proportion of Enstatite and Chrome Diopside

The Cu values of this pyroxenite range from 8 to 33 ppm with an average of 20.5 ppm, Co varies 65 to 87 ppm (average 77 ppm), Ni value from 611 to 823 ppm (average 692 ppm), Cr from 3600 to 5300 ppm (average 4410 ppm). The total Pt + Pd values 27 to 208 ppb (average 103 ppb). Two samples (TE-27 and TE-31) which are collected from the south eastern limb of F-2-fold show high values of total Pt + Pd as 187 and 208 ppb, respectively,

4.1.4. Mineral Chemistry

SEM-EDS Studies were carried out for 15 rock thin sections of pyroxenite and gabbro. Pentlandite [$(Fe, Ni)_9S_8$], Chalcopyrite, Nickel bearing pyrite and galena are the main sulphide phases identified in the samples (Figure 7A,B). Barite, monazite, zircon, and wolframite also occur as discrete traces along with sulphide phases, which indicate that sulphide mineralization might have been contaminated in upper crust with the granophile element [50]. The ultramafic and mafic rocks of Torappadi complex are studied, to assess the mineral-chemical characters of the constituent phases by Electron Micro Probe analysis (EPMA) at GSI, SR, Hyderabad.

4.1.5. Pyroxene

The structural formulae of orthopyroxene and clinopyroxene were calculated on 6 oxygen basis (Supplementary Table S4). The magnesium-iron ratio (Mg#) is particularly useful as an index of crystal fractionation in basaltic liquids [51, 52] and it is calculated in wt% as 100 [MgO/(MgO + FeO)]. The Mg# of orthopyroxene in pyroxenite varies from 79 to 90% and in norite it values from 60 to 61%, clinopyroxene Mg# in pyroxenite range from 86 to 92% and few grains of clinopyroxene occurrence in norite having Mg# of 70%. The Mg# of amphibole occurrences in pyroxenite vary from 83% to 91% and in norite it values from 61% to 62%. The variance of Mg# in pyroxenite and noritic to gabbroic composition rock suggesting variable degrees of crystal fractionation. The value of Mg# in basic rock (gabbroic composition rock) deviates from primitive composition towards more evolved composition. The pyroxenite shows Mg# more than 70% and is interpreted as primitive composition.

When the pyroxene data are plotted in Q (Ca + Mg + Fe^{2+}) − J (2Na) diagram [53], all they occupy QUAD (Ca–Mg–Fe) field (Figure 8A). Similarly, in the ternary Wo-En-Fs diagram, orthopyroxene is plotting in the clinoenstatite and clinopyroxene are clustering in diopside field (Figure 8B) [54]. Compositionally these calcium-poor pyroxenes are enstatite (En 90-79), they significantly lack in exsolution lamellae and Ca-poor corresponding to a subsolvus composition [55]. The exsolution between clinopyroxene and spinel reflects the existence of equilibrium between them during crystallization.

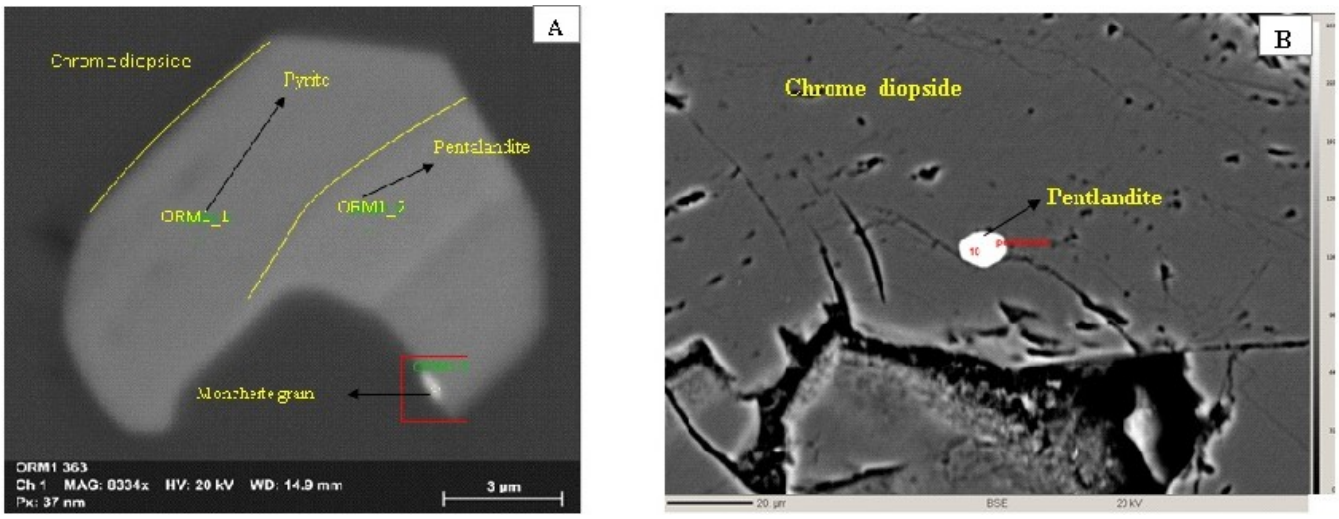

Figure 7. Backscattered electron (BSE) images from SEM-EDS study illustrating (**A**) The association of pyrite (ORM1_1), pentlandite (ORM1_2) and Moncheite (ORM1_3) within the chrome diopside of pyroxenite; (**B**) Sulphide phase pentlandite associated with clinopyroxene (chrome diopside).

4.1.6. Amphibole

The structural formulae for amphiboles were calculated on 23 oxygen basis (Supplementary Table S5), it is found that the amphibole has (Ca + Na)B $\geq$ 1.34 and NaB $<$ 0.67 [44] and hence grouped as calcic amphibole (Figure 9A) [56, 57] which are formed mainly due to the change in the partitioning related to coexisting minerals. The Si vs. Mg/(Mg + Fe^{2+}) diagram [57] shows that the amphiboles from TUC fall in the field of magnesio-hornblende affinity (primary hornblende) (Figure 9B).

4.1.7. Feldspar

The calculated An content for the TUC pyroxenite (websterite) varies from 0.71 to 0.73% and the gabbro shows An content of 57 to 59%. The plagioclase in pyroxenite is bytownite while the gabbro is composed of labradorite variety (Figure 10A and Supplementary Table S6).

4.1.8. Cr-spinel

The chromian spinel shows a large composition variation, in the Cr–Al–Fe^{3+} ternary discrimination diagram [59] (Figure 10B), In TUC, the spinel from diopsidite is classified as Al-chromite while the websterite contains Al-chromite to Cr-spinel (Supplementary Table S7).

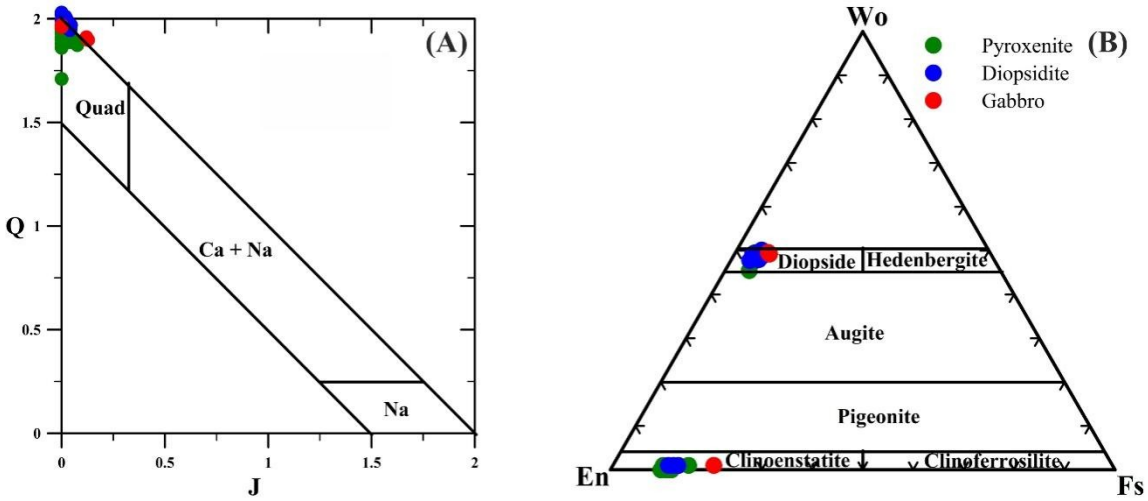

Figure 8. (**A**) Plots of investigated pyroxene composition of Torappadi complex in Q–J diagram [53]; (**B**) Plots of investigated pyroxene composition of Torappadi Ultramafic–Mafic Complex (TUC) in Wo-En-Fs diagram [54].

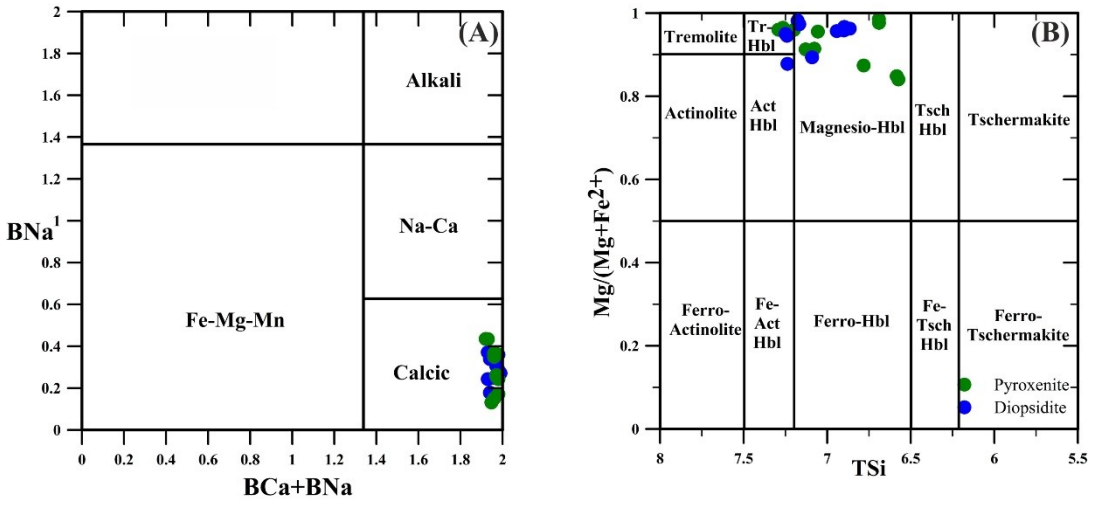

Figure 9. (**A**) Projection of investigated Amphibole compositions of TUC in (Ca + Na) $_B$ versus Na_B diagram [56]; (**B**) Projection of investigated Amphibole compositions of TUC in Si vs. Mg/(Mg + Fe^{2+}) diagram [58].

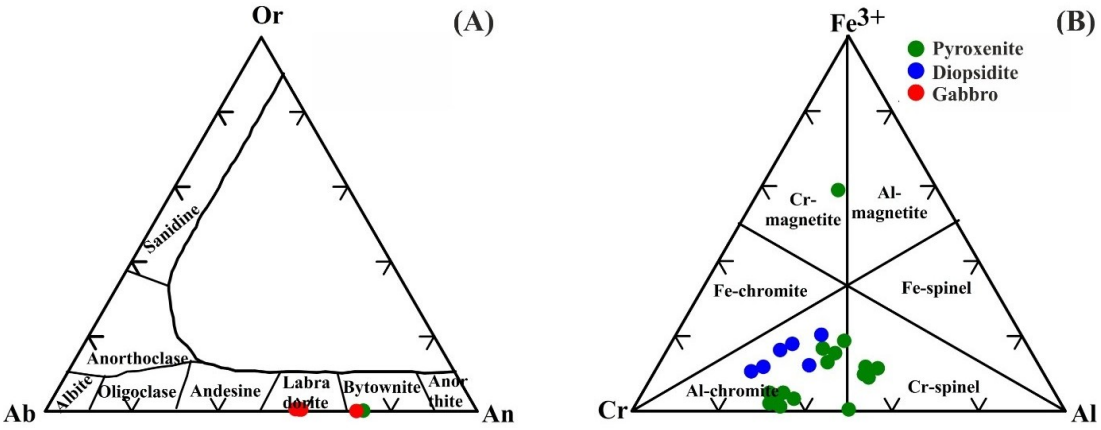

Figure 10. (**A**) Projection of investigated plagioclase compositions in Orthoclase (Or)-Albite (Ab)-Anorthite (An) triangular diagram of TUC; (**B**) Trivalent Cr–Al–Fe^{3+} ternary cation plot of chromium spinel from TUC.

5. Discussion

5.1. Mineralization in TUC

The sulphide phases like pentlandite, chalcopyrite and pyrite occur as sub-microscopic disseminations in pyroxenite and gabbro in association with silicates (chrome diopside). The primary sulphide mineralization is rarely observed even on the freshly broken surface of pyroxenites and gabbro however, fine disseminations are recorded during microscopic study. Samples for PGE analysis were collected mainly from the variants of pyroxenite and gabbro. The ΣPGE values of 145 samples are ranging between 14 ppb and 380 ppb. Out of 145, 34 samples were analyzed more than 100 ppb of ΣPGE of which 30 samples are from enstatite rich pyroxenite variety while three samples belong to chrome-diopside rich pyroxenite and one sample pertains to diopsitite. Moreover, when the data are plotted over the geological map of TUC, it is apparent to notice that the samples with more than 100 ppb of ΣPGE are clustering around the hinges of the F_1 and F_2 folds (Figure 2). The bivariate plots of Ni vs. Cr for representative samples of pyroxenite (with ΣPGE >100 ppb) indicating that Ni is showing sympathetic variation and positive slope with Cr indicating the primary fractionation trends (Figure 11). Whereas, Cu, Pt and Pd show non-sympathetic relation with Ni indicating the restricted redistribution of PGE during D1 and D2 deformational event which was substantiated by the elevated ΣPGE (>100 ppb) of the samples from around fold hinges.

5.1.1. REE Geochemistry

The pyroxenites display a wide range of ΣREE (8–1021 ppm), LREE/HREE (0.57–4.23), LaN/SmN (0.58–6.10), and GdN/YbN (0.08–6.69), indicating significant decoupling between LREE, MREE, and HREE (Figure 12A) [60, 61]. The uniform high LaN/SmN ratios (∼6.1) in several samples reflect preservation of a primary LREE-enriched magmatic cumulate signature [62, 63] while wide variation and pronounced scattering in GdN/YbN and LaN/YbN ratios (Figure 12C), together with variable Eu anomalies, indicates selective redistribution of MREE and HREE. Samples with low LaN/SmN (<1) and anomalously high or low GdN/YbN are inferred to indicate deformation-assisted fluid–rock interaction resulting in selective redistribution of REE without complete resetting of the primary magmatic signature [63–65].

The chondrite-normalized REE patterns of the gabbros are characterized by low to moderate total REE contents, relatively flat HREE patterns, and pronounced positive Eu anomalies ($Eu/Eu^* = 2.8–10.9$) (Figure 12B). Such features are typical of plagioclase-rich gabbroic cumulates, where Eu^{2+} is preferentially incorporated into plagioclase during crystallization. The limited range of LREE/HREE (0.47–1.87) and moderate LaN/YbN ratios (0.77–4.78) indicate closed-system magmatic differentiation with minimal post-magmatic modification (Figure 12C). Overall, the REE systematics of the gabbro reflects primary magmatic processes dominated by plagioclase and clinopyroxene fractionation [60, 62, 66].

5.1.2. PGE and Trace Element Geochemistry

The primitive mantle–normalized Ni–Cu–PGE patterns of the pyroxenites and gabbro samples of TUC are characterized by moderate depletion of Ni and Co, a pronounced negative Ir anomaly and a gradual enrichment from IPGE (Ir–Ru–Rh) to PPGE (Pt–Pd), with relative enrichment of Cu (Figure 12D,E). Such fractionated PGE patterns indicate that these rocks formed from an evolved mafic magma that experienced early silicate fractionation and sulfide saturation [65]. Depletion of Ni and Co reflects their compatible behavior during early crystallization of olivine and clinopyroxene, whereas the strong Ir depletion suggests early segregation of monosulfide solid solution (MSS), which preferentially scavenges IPGE, followed by enrichment of Pt, Pd and Cu in a residual, Cu-rich sulfide melt during advanced stages of magmatic differentiation [22, 65, 67]. Such fractionated PGE patterns are characteristic of magmatic sulfide fractionation processes in layered mafic–ultramafic systems and argues against significant post-magmatic hydrothermal remobilization [68, 69].

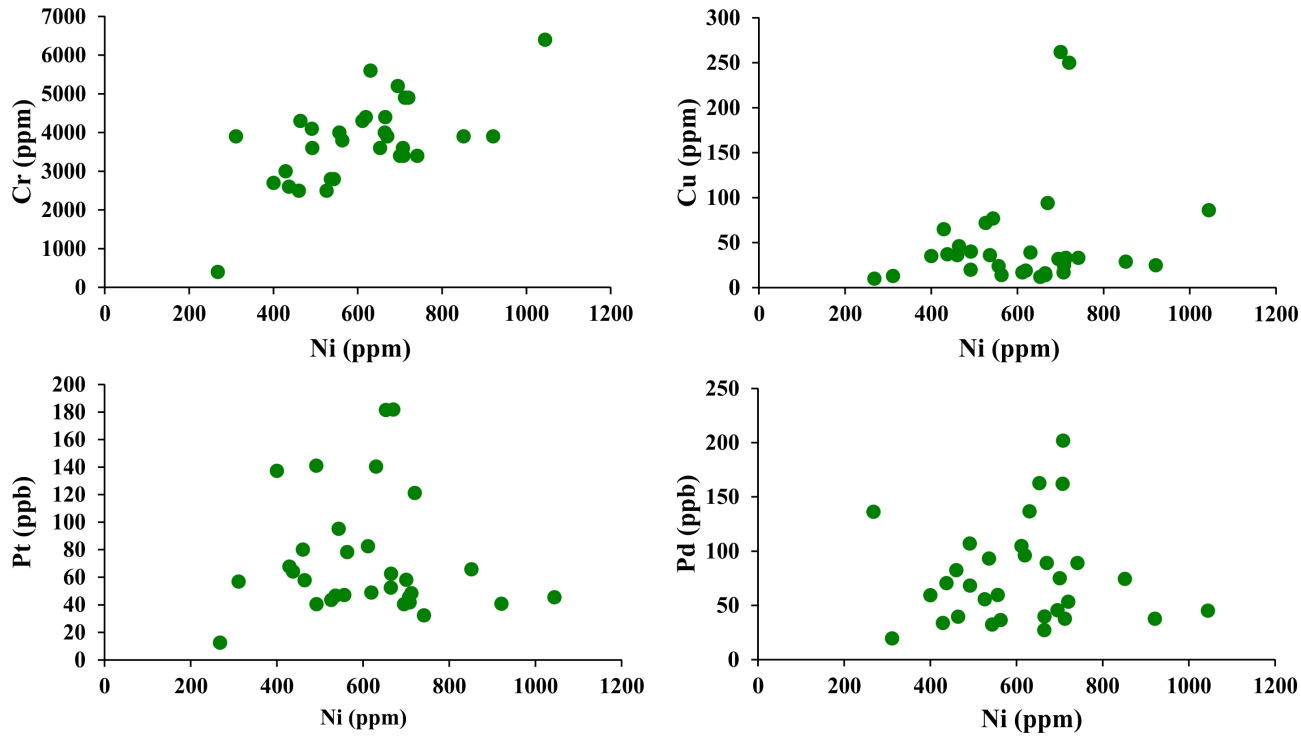

Figure 11. Bivariate plots of Ni vs. Cr, Cu, Pt and Pd of pyroxenite of TUC (pyroxenite samples with >100 ppb of ΣPGE are plotted).

5.1.3. Controls on PGE Distribution

(i) Pd vs. Cu/Pd

The Pd vs. Cu/Pd discrimination plot delimits depleted and undepleted magma characteristics. A cluster of gabbroic and pyroxenite samples of TUC show high Cu/Pd (>1000) and low Pd (<50 ppb) and a separate population of diopsidite–ortho-pyroxenite samples trending to low Cu/Pd (<1000) and elevated Pd (>50 ppb) (Figure 13A). The former likely reflects either late-stage Pd depletion by early sulphide segregation [70, 71], whereas the latter indicates localized Pd enrichment likely due to later stage crystallization or differentiation processes where Pd is concentrated [72, 73].

Therefore, the inverse relationship and overlapping signatures in the Pd versus Cu/Pd plot suggest the evolving trend of the single parental magma with progressive differentiation instead of episodic nature of different magma pulses. Consequently, the samples plotting in the high Pd and low Cu/Pd field may signify the potential targets for PGE, whereas detailed base-metal (Cu–Ni) sulphide investigation along with isotopic investigation to be carried out for the Cu-rich group.

(ii) Cu vs. Pd

This plot illustrates the relationship copper (Cu) with palladium (Pd) in pyroxenite variants and gabbro of the TUC for understanding the impact of sulfur (S) saturation and sulfur-under saturation (Figure 13B). If the sulfur is sufficiently enriched in the magma to form immiscible sulfide phases, the melt will be concentrated with palladium and other PGEs. These plots show the bimodal distribution of TUC samples where, the pyroxenites, ortho-pyroxenites, and gabbro samples plotting in the sulfur saturation field suggesting the removal of PGEs (such as Pd) from the silicate melt due to early sulfur saturation [70]. On the other hand, diopsidite and gabbro in the S-undersaturated region indicate that the sulfur was insufficient in the environments to form sulfide phases, resulting in the retention and enrichment of PGE, particularly Pd in the system. As reported from other studies, sulfur saturation is the key factor for influencing the PGE mineralization in mantle derived magmas [70, 72, 73].

(iii) Ni/Cu vs. Pd/Ir

The Ni/Cu vs. Pd/Ir is an effective discrimination diagram for characterizing various magmatic processes (source, fractional crystallization, and sulphide immiscibility) which control the distributions of PGE and base-metals in the system [6, 22]. In this diagram, Ni/Cu primarily records the relative compatibility of Ni against Cu during early olivine/chromite crystallization and sulphide segregation, whereas Pd/Ir tracks fractionation between PPGE (Pd, Pt) and IPGE (Ir, Os) and thus records the relative removal or retention of Pd in any sulphide phase [6, 74].

The data cluster in the central-right portion of the diagram, overlapping the ophiolite / chromitite / layered intrusion fields and trending toward the PGE-reef domain (Figure 14). This distribution indicates a dominantly mantle-derived, high-Mg (ultramafic) parental magma that experienced variable fractional crystallization and episodic sulphide immiscibility. Magmas that remain S-undersaturated

during early crystallization permit Pd and other PPGE to remain concentrated in the residual silicate melt (promoting reef-type PGE enrichment), whereas early S-saturation and sulphide segregation removes Pd into sulfides and shifts samples toward low Pd/Ir [7, 75]. The observed spread from mantle/komatiite fields into the PGE-reef field therefore records episodes of Pd enrichment in residual melts followed by varying degrees of sulphide segregation.

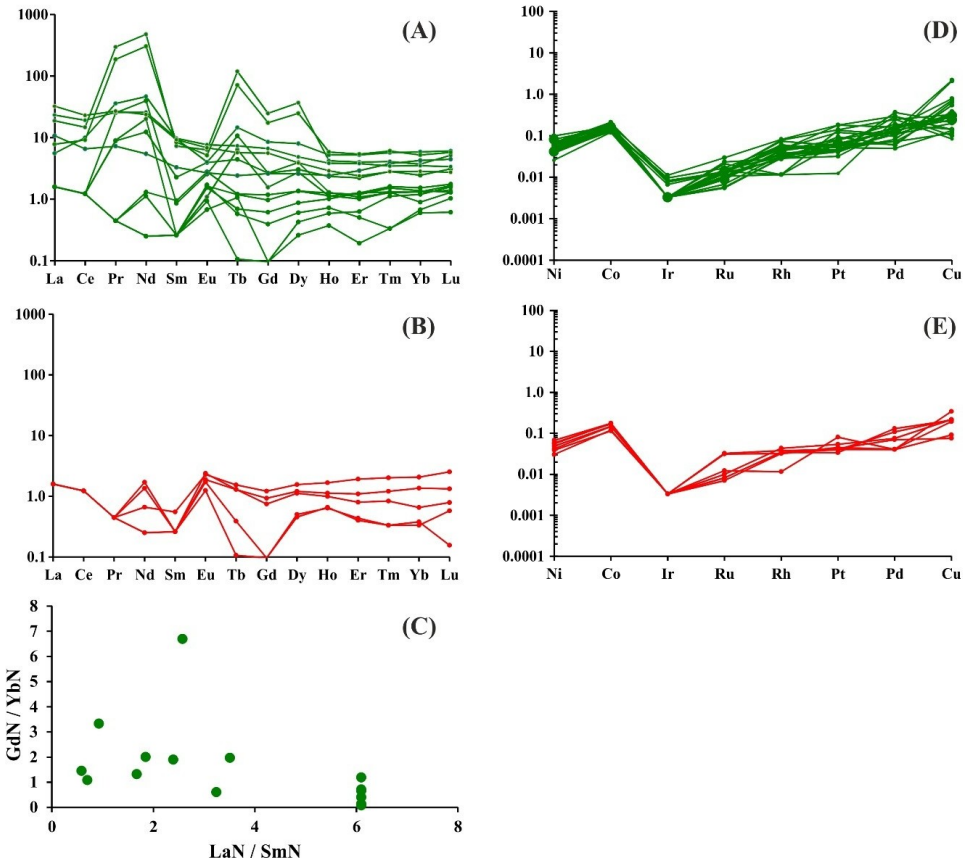

Figure 12. (**A**) Chondrite-normalized rare earth element (REE) plot for pyroxenite of Torappadi Ultramafic–Mafic Complex (TUC) indicates the preservation primary magmatic cumulate signature. Normalizing factor are from [62]; (**B**) Chondrite-normalized REE plot of gabbro from TUC showing low fractionation of LREE with flat HREEs; (**C**) LaN/SmN vs. GdN/YbN plot for pyroxenites of TUC suggesting the localized post-magmatic modification; (**D**) Primitive mantle-normalized [62] spider diagram of PGEs plus Ni, Co, and Cu for pyroxenite and (**E**) Gabbro samples of TUC highlighting gradual enrichment from IPGE (Ir–Ru–Rh) to PPGE (Pt–Pd).

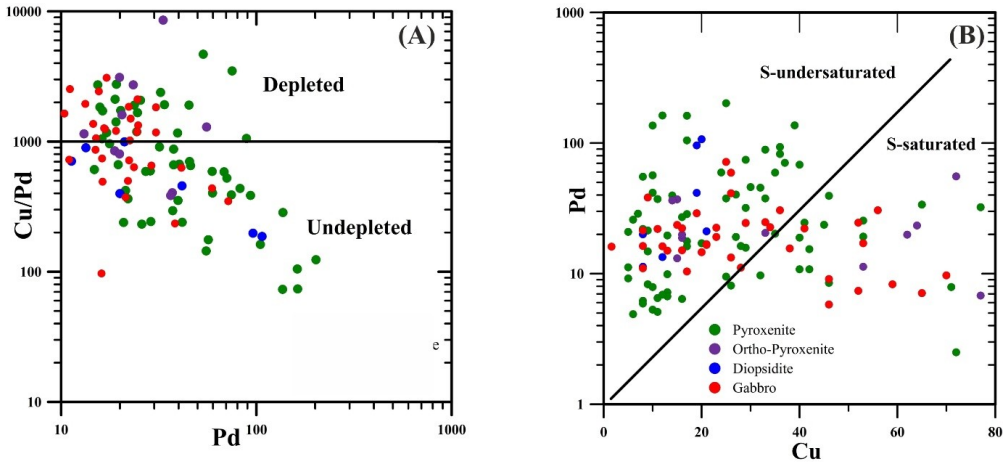

Figure 13. (**A**) Plot of Cu versus Cu/Pd for ultramafic–mafic rocks of TUC indicating it's undepleted to depleted nature; (**B**) Cu versus Pd discrimination figure for Torappadi ultramafic–mafic rocks showing bimodal nature of magmatic environment. The dividing line of S-saturation is after [76].

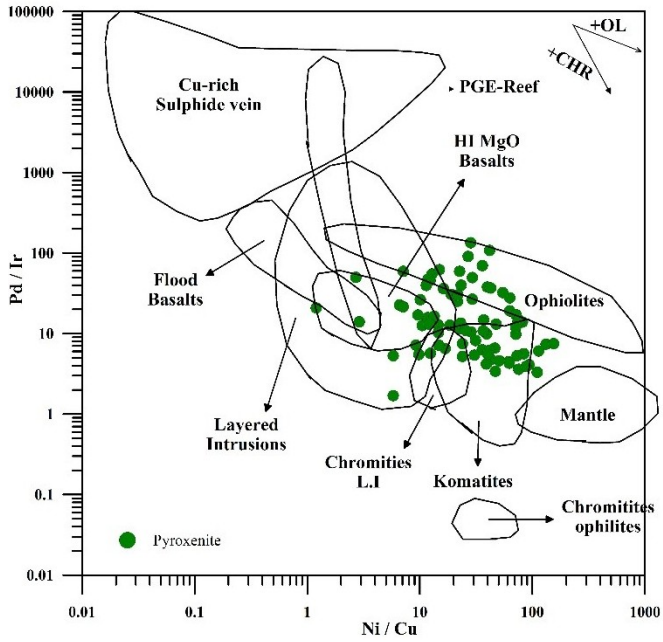

Figure 14. Discrimination diagram (modified after [17]) of Ni/Cu vs. Pd/Ir for ultramafic pyroxenites of Torappadi Ultramafic–Mafic Complex showing that the TUC pyroxenites are plotting in layered intrusion to komatiite field.

The discrimination plots, Pd vs. Cu/Pd; Cu vs. Pd and Ni/Cu vs. Pd/Ir, substantiate that the PGE mineralization evolved under a dynamic magmatic condition relating to: (a) initial mantle derived magma with high Mg content and potential of chalcophile element; (b) variable sulfur saturation: locally early saturation led to Pd depletion, while elsewhere, prolonged S-undersaturation allowed Pd enrichment; and (c) fractional crystallization and melt differentiation caused Pd and Pt accumulation in late-stage silicate melts, producing reef-type mineralization in pyroxenite–orthopyroxenite units.

Low sulphur-fugacity magmas have potential to enrich PGE, relative to the Cu in the system and most magmatic Ni–Cu and PGE deposits around the world that are formed from sulfide-undersaturated silicate magmas [67, 77]. Relation of Cu with the Pd in Cu vs. Pd and Pd vs. Cu/Pd plots indicate the degree of partial melting, episodic emplacement of magma and sulphur saturation [17]. Many PGE rich intrusions such as Gondpipri layered intrusion [28], Sukinda Massif [32], Bushveld [78], Norilsk [2] have resulted from the strongly S-undersaturated parental magma. On the other hand, sulfide saturation early in the parental magma results incongruous for segregation of PGE in the system and thus economically viable PGE deposits would not form [8]. Therefore, continuous and overlapping trend of depleted to undepleted and S-undersaturated to S-saturated signatures observed in the Pd versus Cu/Pd plots of TUC signify the progressive in-situ differentiation of a single evolving parental magma, rather than emplacement of distinct magma pulses.

6. Conclusion

The TUC is characterized by high Mg, low calcic and low alkali litho-assemblages of komatiitic field trend. Our study revealed high ΣPGE content of up to 380 ppb in the pyroxenite and diopsidite whereas the gabbro shows relatively lower ΣPGE content of up to 117 ppb. Even though sulphide phases like pentlandite, chalcopyrite and pyrite are identified in the pyroxenite through SEMEDS and EPMA studies, the PGE phases are associated with the silicate phases especially within chrome diopside. This evidence indicates that the magma remained S-undersaturated during early crystallization allowing Pd and other PPGE to remain concentrated in the residual silicate melt. Integrated geochemical signatures of PGE, trace elements and REE indicate that the primary magmatic differentiation and early sulphur fractionation influenced the segregation of PGE in the system while the subsequent deformation assisted fluid–rock interaction resulted selective redistribution of PGE around structural closures.

The PGE potential in Torappadi Ultramafic–Mafic Complex is significant, particularly in pyroxenite and orthopyroxenite cumulate layers that record low Cu/Pd, high Pd/Ir, and S-undersaturated conditions. In contrast, Cu-rich and S-saturated pyroxenites are more prospective for Cu–Ni sulfide mineralization but are less PGE-enriched. The lithology as well as structural control over the PGE distribution in TUC suggests prudent selection of exploration targets for future.

Supplementary Materials

The supporting information can be downloaded at: https://media.sciltp.com/articles/others/2603161521042752/ESRS-25110112-SM.pdf.

Author Contributions

V.S.: Field work; Conceptualization; Data curation; Formal analysis; Investigation; Methodology; Writing—original draft and editing; V.K.: Conceptualization; Methodology; Writing—review & editing; J.P.: Writing—review & editing; S.S.C.: Writing—review & editing; Conceptualization; P.D.: review & editing; Y.B.: Field work; Data curation. All authors have read and agreed to the published version of the manuscript.

Funding

This research received no external funding.

Institutional Review Board Statement

Not applicable.

Informed Consent Statement

Not applicable.

Data Availability

The data presented as results in this manuscript are not available anywhere else. However, the original data used in this article are available upon request to the corresponding author.

Acknowledgements

The authors express their sincere gratitude to Shri Basab Mukhopadhyay, Additional Director General and Head of Department, Southern Region, Geological Survey of India (GSI), Hyderabad, and Shri Bonthu Ajaya Kumar, Deputy Director General, GSI, State Unit: Tamil Nadu & Puducherry, Chennai for providing the necessary logistic support for fieldwork and sample collection and permission to carry out this research work. S.B. Vijay Kumar and G. Nagendran, GSI, SU: TN&P, Chennai, and N.P. Nathan, GSI acknowledged for their constructive discussions that greatly contributed to improving the quality of this work. The authors also gratefully to the Chemical Division, Petrological Division and Palaeontology Division, GSI, Southern Region, Hyderabad, for their support in carrying out the chemical analyses, EPMA and SEM–EDS studies. Authors profusely thank the Editors-in-Chief, Joseph G. Meert, and M. Santosh and the reviewers M.L. Dora and Jaganmoy Jodder for providing insightful comments and constructive suggestions for improving the quality of the manuscript.

Conflicts of Interest

The authors declare that they have no known competing financial interests or personal relationships that could have appeared to influence the work reported in this paper Given his role as Associate Editor of this Journal. Dr. S.S. Chinnasamy had no involvement in the peer review of this article and had no access to information regarding its peer review. Full responsibility for the editorial process for this article was delegated to another journal editor.

Use of AI and AI-assisted Technologies

The authors used Grammarly English correction Tool during the preparation of this manuscript. After that, the authors reviewed and edited the content as needed and take full responsibility for the content of the publication.

References

1. Cameron, D.S. Fuel cell energy generators. *Platin. Met. Rev.* **1978**, *22*, 38–46.
2. Naldrett, A.J.; Duke, J.M. Platinum metals in magmatic sulfide ores. *Science* **1980**, *208*, 1417–1424.
3. Cabri, L.J. The platinum-group minerals. In *Platinum-Group Elements: Mineralogy, Geology, Recovery*; Cabri, L.J., Ed.; Canadian Institute of Mining and Metallurgy: Montreal, QC, Canada, 1981; Special Volume 23, pp. 83–150.
4. Cabri, L.J. The platinum-group minerals. In *The Geology Geochemistry, Mineralogy and Mineral Beneficiation of Platinum-Group Elements*; Cabri, L.J., Ed.; Canadian Institute of Mining and Metallurgy: Montreal, QC, Canada, 2003; Special Volume 41, pp. 544–546. https://doi.org/10.2113/gscanmin.41.2.544
5. Buchanan, D.L. *Platinum-group Element Exploration, Developments in Economic Geology*; Elsevier Science Publishers: New York, NY, USA, 1988; p. 184.
6. Barnes, S.J.; Naldrett, A.J.; Gorton, M.P. The origin of the fractionation of the platinum-group elements in terrestrial magmas. *Chem. Geol.* **1985**, *53*, 303–323. https://doi.org/10.1016/0009-2541(85)90076-2
7. Qing, L.; Quanlin, H.; Liewen, X.; et al. Different origins of the fractionation of platinum-group elements in Raobazhai and Bixi Ling mafic rocks from Dabie Orogen, Central China. *J. Geol. Res.* **2012**, *2012*, 631426. https://doi.org/10.1155/2012/631426
8. Maier, W.D. Platinum-group element (PGE) deposits and occurrences: Mineralization styles, genetic concepts, and exploration criteria. *J. Afr. Earth Sci.* **2005**, *41*, 165–191. https://doi.org/10.1016/j.jafrearsci.2005.03.004
9. Mondal, S.K.; Zhou, M.F. Enrichment of PGE through interaction of evolved boninitic magmas with early formed cumulates in a gabbro-breccia zone of the Mesoarchean Nuasahi massif (Eastern India). *Miner. Depos.* **2010**, *45*, 69–91. https://dx.doi.org/10.1007/s00126-009-0264-0
10. Barnes, S.J.; Lightfoot, P.C. Formation of magmatic Ni–Cu–PGE sulphide deposits and processes affecting their Cu and PGE contents. In *Economic Geology 100th Anniversary* Volume; Economic Geology Publishing Company: Littleton, CO, USA, 2005; pp. 179–213. https://doi.org/10.5382/AV100
11. Hudson, D.R.; Robinson, B.W.; Vigers, R.B.W.; et al. Zoned michenerite testibiopalladite from Kambalda, Western Australia. *Can. Mineral.* **1978**, *16*, 121–126.
12. Naldrett, A.J.; Wilson, A.; Kinnaird, J.; et al. PGE tenor and metal ratios within and below the Merensky Reef, Bushveld Complex: Implications for its genesis. *J. Petrol.* **2009**, *50*, 625–659.
13. Crocket, J.H.; Paul, D.K. Platinum-group elements in Deccan mafic rocks: A comparison of suites differentiated by Ir content. *Chem. Geol.* **2004**, *208*, 273–291.
14. Chen, G.; Xia, B. Platinum-group elemental geochemistry of mafic and ultramafic rocks from the Xigaze ophiolite, Southern Tibet.

J. Asian Earth Sci. **2008**, *32*, 406–422. https://doi.org/10.1016/j.jseaes.2007.11.009

15. Brain, D.G. Igneous Petrology of the Ni–Cu–PGE Mineralised Tamrack Intrusion, Aitkin and Carlton Counties, Minnesota, Master's Thesis, University of Minnesota, Minnesota, 2011. https://hdl.handle.net/11299/104139
16. Randine, K.; Kumar, J.V.; Korakoppa, M. Platinum-group elements mineralization in the cumulate gabrro of Phenai Mata complex, Deccan Large Igneous Province, India. *Curr. Sci.* **2015**, *108*, 1796–1798.
17. Barnes, S.J. The use of metal ratios in prospecting for platinum group elements deposits in mafic and ultramafics intrusions. *J. Geochem. Explor.* **1990**, *37*, 91–99. https://doi.org/10.1016/0375-6742(90)90084-N
18. Dare, S.A.A.; Barnes, S.J.; Prichard, H.M. The distribution of platinum group elements (PGE) and chalcophile elements among sulfides from the Creighton Ni–Cu–PGE sulfide deposit, Sudbury, Canada, and the origin of palladium in pentlandite. *Miner. Depos.* **2010**, *45*, 765–793. https://doi.org/10.1007/s00126-010-0295-6
19. Maier, W.D.; Barnes, S.J.; Chinyepi, G.; et al. The composition of magmatic Ni-Cu-(PGE) sulfide deposits in the Tati and Selebi-Phikwe belts of eastern Botswana. *Miner. Depos.* **2008**, *43*, 37–60. https://doi.org/10.1007/s00126-007-0143-5
20. Maier, W.D.; Barnes, S.J.; Sarkar, A.; et al. The Kabanga Ni Sulfide deposit, Tanzania: 1. Geology, petrography, silicate rock geochemistry, and sulfur and oxygen isotopes. *Miner. Depos.* **2010**, *45*, 419–441. https://doi.org/10.1007/s00126-010-0280-0
21. Godel, B.; Barnes, S.J.; Maier, W.D. Platinum-group-elements in sulphide minerals, platinum-group minerals, and whole-rocks of the Merensky Reef (Bushveld Complex, South Africa): Implications for the formation of the reef. *J. Petrol.* **2007**, *48*, 1569–1604. https://doi.org/10.1093/petrology/egm030
22. Naldrett, A.J. *Magmatic Sulfide Deposits: Geology, Geochemistry and Exploration*; Springer-Verlag: Berlin and Heidelberg, Germany, 2004; p. 727. https://doi.org/10.1007/978-3-662-08444-1
23. Pina, R.; Gervilla, F.; Ortega, L.; et al. Mineralogy and geochemistry of platinum-group elements in the Aguablanca Ni–Cu deposit (SW Spain). *Miner. Petrol.* **2008**, *92*, 259–282. https://doi.org/10.1007/s00710-007-0195-3
24. Gorbunov, G.I. *Geology and Genesis of the Pechenga Ni–Cu Sulfide Deposits*; Nedra: Moscow, Russia, 1968; p. 352. (In Russian).
25. Ross, J.R.; Hopkins, G.M.F. Kambalda nickel sulphide deposits. In *Economic Geology of Australia and Papua-New Guinea, Metals*; Knight, C.L., Ed.; Australasian Institute of Mining and Metallurgy Monograph Series; Australasian Institute of Mining and Metallurgy: Parkville, VIC, Australia, 1975; Volume 5, pp. 100–121.
26. Boudreau, A.E.; Mathez, E.A.; McCallum, I.S. Halogen geochemistry of the Stillwater and Bushveld complexes: Evidence from hydrous silicates and fluid inclusions. *J. Petrol.* **1986**, *27*, 967–986.
27. Auge, T.; Cocherie, A.; Genna, A.; et al. Age of Baula PGE mineralization (Orissa, India) and its implications concerning the Singhbhum Archean Nucleus. *Precambrian Res.* **2003**, *121*, 85–101. https://doi.org/10.1016/S0301-9268(02)00202-4
28. Mondal, S.K.; Khatun, S.; Prichard, H.M.; et al. Platinum Group Elements geochemistry of boninite derived Mesoarchaean chromitite and ultramafic-mafic cumulate rocks from the Sukinda Massif (Orissa, India). *O. Geol. Rev.* **2019**, *104*, 722–744. https://doi.org/10.1016/j.oregeorev.2018.11.027
29. Dora, M.L.; Meshram, T.; Baswani, S.R.; et al. The Paleo-Mesoarchaean Gondpipri mafic-ultramafic intrusions, western Bastar Archaean Craton, Central India: Insights from bulk-rock geochemistry and Sm–Nd and S isotope studies on the formation of Ni–Cu–PGE mineralization. *Econ. Geol.* **2022**, *117*, 1845–1866.
30. Farooqui, S.A.; Singh, A.K. Platinum mineralization in Ikauna area, Lalitpur district, Uttar Pradesh. *J. Geol. Soc. India* **2006**, *68*, 582–584. https://doi.org/10.17491/jgsi/2006/680403
31. Allapieti, T.T.; Devaraju, T.C.; Kaukonen, R.J. PGE mineralisation in the Late Archean iron rich mafic-ultramafic Hanumalapur complex, Karnataka, India. *Miner. Petrol.* **2008**, *92*, 99–128. https://doi.org/10.1007/s00710-007-0211-7
32. Sesha Sai, V.; Nathan, N.P.; Kumar, R.; et al. Occurrence of PGE minerals in Archaean Sittampundi layered anorthosite complex, Tamil Nadu, south India. *Indian Miner.* **2009**, *63*, 305–310.
33. Nathan, N.P.; Vijay Kumar, R.; Prabhakar, J.; et al. *Exploration for Platinum Group of Elements in India, Special Publication No. 122*; Geological Survey of India: Kolkata, India, 2022; p. 170.
34. Indian Bureau of Mines. *Indian Minerals Yearbook*; Indian Bureau of Mines: Nagpur and Delhi, India, 2007.
35. Dora, M.L.; Singh, H.; Kundu, A.; et al. Tsumoite (BiTe) and associated Ni-PGE mineralization from Gondpipri mafic-ultramafic complex, Bastar craton, Central India: Mineralogy and genetic significance. *Central Eur. J. Geosci.* **2014**, *6*, 506–517.
36. Singh, S.; Balaram, V.; Satyanarayanan, M.V.; et al. Platinum group elements in basic and ultrabasic rocks around Madawara, Bundelkhand Massif, Central India. *Curr. Sci.* **2010**, *99*, 375–383.
37. Dora, M.L.; Nair, K.K.K.; Shasidharan, K. Occurrence of platinum group minerals in the Western Bastar Craton, Chandrapur District, Maharashtra. *Curr. Sci.* **2011**, *100*, 399–404.
38. Mondal, R.; Baidya, T. Titaniferous magnetite deposits associated with Archean Greenstone belt in the East Indian shield. *Earth Sci.* **2015**, *4*, 15–30. https://doi.org/10.11648/j.earth.s.2015040401.12
39. Majumdar, D.; Gogoi, A. First report on platinum occurrence in ultramafic-mafic complex, East-Central Karbi Hills of Assam, North East India. *J. Geol. Soc. India* **2019**, *94*, 245–248. https://doi.org/10.1007/s12594-019-1303-9
40. Subramaniam, A.P. Mineralogy and petrology of the Sittampundi Complex, Salem district, Madras State, India. *Bull. Geol. Soc. Am.* **1956**, *67*, 317–390. http://dx.doi.org/10.1130/0016-7606(1956)67[317:MAPOTS]2.0.CO;2
41. Gopalakrishnan, R. *Reconnaissance Survey for Platinum Group of Elements in Torappadi-Ponakkadu area, Tiruvannamalai–Sambuvarayar District, Tamil Nadu*; Geological Survey of India: Tamil Nadu, India, 1999. (Unpublished Report)
42. Ray, J. Mineral Chemistry of mafic chain silicate minerals in the Torappadi layered complex of the Southern Granulite Terrain. *J. Geol. Soc. India* **1995**, *45*, 531–537.
43. Ray, J.S.; Bose, M.K. Occurrence of ultramafic rocks in Torappadi layered complex, North Arcot district, Tamil Nadu. *Indian Miner.* **1993**, *47*, 195–206.
44. Ray, J. Structure and Petrology of Torappadi Igneous Complex and Surrounding Area, Arcot District, Tamil Nadu. Ph.D. Thesis, University of Calcutta, Calcutta, India, 1988.
45. Sugavanam, E.B. *Geology of Parts of Chengam and Thiruvannamalai Taluks, North Arcot District, Tamil Nadu*; Geological Survey of India: Tamil Nadu, India, 1973. (Unpublished Report)
46. Venkata Rao, V. *Report on the Geological and Structural and Petrological Studies of Parts of Ultramafic Complex Near Torappadi, North Arcot District, Tamil Nadu*; Geological Survey of India: Tamil Nadu, India, 1975. (Unpublished Report)
47. Velladurai, S.; Bhogta, Y. *Reconnaissance Survey for Platinum Group of Elements (PGE) in Torappadi Ultramafic Complex, Tiruvanamalai District, Tamil Nadu*; Geological Survey of India: Tamil Nadu, India, 2017. (Unpublished Report)
48. Sowminarayanan, V.R.; Srinivasan, B.V.; Maharaja Singh, H.J. *Geochemical and Second Generation Geological Mapping of the Alkaline – Carbonatite Complex Around Bommikuppam – Kambugudi – Kavalur – Kallatur Areas, Tiruppattur and Chengam Taluks, North Arcot District, Tamil Nadu*; Geological Survey of India: Tamil Nadu, India, 1994. (Unpublished Report)
49. Jensen, L.S. *A New Cation Plot for Classifying Subalkalic Volcanic Rocks*; Ontario Division Mines, Miscellaneous Paper 66; Ontario Department of Mines: Toronto, ON, Canada, 1976; p. 22.

50. Maier, W.D.; Barnes, S.J.; Sarkar, A.; et al. The kabanga Ni sulfide deposit, Tanzania: I. Geology, petrography, silicate rock geochemistry, and sulfur and oxygen isotopes. *Miner. Depos.* **2010**, *45*, 419–441.
51. Oskarsson, N.; Sigvaldson G.E.; Steinthorsson S. A dynamic model of rift zone petrogenesis and the regional petrology of Iceland. *J. Petrol.* **1982**, 23, 28–74.
52. Wilkinson, J.F.G. The genesis of mid-ocean ridge basalt. *Earth Sci. Rev.* **1982**, *18*, 1–57. https://doi.org/10.1016/0012-8252(82)90002-2
53. Morimoto, N. Nomenclatures of pyroxenes. *Can. Mineral.* **1989**, *27*, 143–156.
54. Poldervaart, A.; Hess, H.H. Pyroxenes in the crystallization of basaltic magmas. *J. Geol.* **1951**, *59*, 472–489. https://doi.org/10.1086/625891
55. Deer, W.A.; Howie, R.A.; Zussman, J. *Rock Forming Minerals*; Geological Society of London: London, UK, 1978; p. 668.
56. Leake, B.E. Nomenclature of amphiboles. *Min. Mag.* **1978**, *42*, 533–56.
57. Kamineni D.C. Distribution of uranium, thorium, and rare earth elements in the Eye Dashwa Lakes pluton. A study of some analogue elements. *Chem. Geol.* **1986**, *55*, 361–373. https://doi.org/10.1016/0009-2541(86)90036-7
58. Leake, B.E. The relationship between composition of calciferous amphibole and grade of metamorphism. In *Controls of Metamorphism*; Pitcher, W.S., Flynn, G.W., Eds.; Oliver and Boyd: Edinburgh, London, UK, 1965; pp. 299–318.
59. Stevens, R.E. Composition of some chromites of the western Hemisphere. *Am. Mineral.* **1944**, *29*, 1–34.
60. Rollinson, H.R. *Using Geochemical Data: Evaluation, Presentation, Interpretation*; Longman Scientific & Technical: Harlow, Essex, UK, 1993; p. 352.
61. Bau, M. Controls on the fractionation of isovalent trace elements in magmatic and aqueous systems: Evidence from Y/Ho, Zr/Hf, and lanthanide tetrad effect. *Contrib. Mineral. Petrol.* **1996**, *123*, 323–333. https://doi.org/10.1007/s004100050159
62. McDonough, W.F.; Sun, S. The composition of the Earth. *Chem. Geol.* **1995**, *120*, 223–253. https://doi.org/10.1016/0009-2541(94)00140-4
63. Ionov, D.; Savoyant, L.; Dupuy, C. Application of the ICP-MS Technique to trace element analysis of peridotites and their minerals. *Geostand. Newsl.* **1992**, *16*, 311–315. https://doi.org/10.1111/j.1751-908x.1992.tb00494.x
64. Bodinier, J.L.; Godard, M. Orogenic, ophiolitic, and abyssal peridotites. In *Treatise on Geochemistry*; Holland, H.D., Turekian, K. K., Ed.; Elsevier: Oxford, UK, 2003; Volume 2, pp. 103–170. https://doi.org/10.1016/B0-08-043751-6/02004-1
65. Barnes, S.; Lightfoot P. Formation of magmatic nickel sulfide deposits and processes affecting their copper and Platinum Group Element. In *Economic Geology 100th Anniversary Volume*; Economic Geology Publishing Company: Littleton, CO, USA, 2005; pp. 179–213. https://doi.org/10.5382/AV100.08
66. Winter, J.D. *Principles of Igneous and Metamorphic Petrology*, 2nd ed.; Prentice Hall: Upper Saddle River, NJ, USA, 2010.
67. Barnes, S.J.; Cox, R.A.; Zientek, M.L. Platinum-group element, Gold, Silver and Base Metal distribution in compositionally zoned sulfide droplets from the Medvezky Creek Mine, Noril'sk, Russia. *Contrib. Mineral. Petrol.* **2006**, *152*, 187–200. https://doi.org/10.1007/S00410-006-0100-9
68. Barnes, S.J; Maier, W.D. The fractionation of Ni, Cu and the noble metals in silicate and sulfide liquids. In *Dynamic Processes in Magmatic Ore Deposits and their Application in Mineral Exploration*; Geological Association of Canada: St. John's, Newfoundland and Labrador, Canada, 1999, Short Course Volume 13, pp. 69–106.
69. Lorand J.P.; Alard, O. Determination of selenium and tellurium concentrations in Pyrenean peridotites (Ariége, France), new insight into S/Se/Te systematics of the upper mantle. *Chem. Geol.* **2010**, *278*, 120–130. https://doi.org/10.1016/j.chemgeo.2010.09.007.
70. Mungall. J.E.; Hanley J.J.; Arndt N.T.; et al. Evidence from meimechites and other low-degree mantle melts for redox controls on mantle-crust fractionation of platinum-group elements. *Proc. Natl. Acad. Sci. USA* **2006**, *103*, 12695–12700. https://doi.org/10.1073/pnas.0600878103
71. Park, JW.; Campbell, I.H.; Malaviarachchi, S.P.K.; et al. Chalcophile element fertility and the formation of porphyry Cu ± Au deposits. *Miner. Depos.* **2019**, *54*, 657–670. https://doi.org/10.1007/s00126-018-0834-0
72. Smythe Duane, J.; Wood Bernard, J.; Kiseeva Ekaterina, S. The S content of silicate melts at sulfide saturation: New experiments and a model incorporating the effects of sulfide composition. *Am. Mineral.* **2017**, *102*, 795–803. https://doi.org/10.2138/am-2017-5800CCBY
73. Cooke, D.R.; Hollings. P.; Wilkinson, J.J.; et al. *Geochemistry of Porphyry Deposits. Treatise on Geochemistry*, 2nd ed.; Elsevier: Oxford, UK, 2014. https://doi.org/10.1016/B978-0-08-095975-7.01116-5
74. Maier, W.D.; Barnes, S.J.; de Waal, A. Exploration for magmatic Ni-Cu-PGE sulphide deposits; a review of recent advances in the use of geochemical tools, and their application to some South African ores. *S. Afr. J. Geol.* **1998**, *101*, 237–253.
75. Li, C.; Ripley, E.M. Empirical equations to predict the sulfur content of mafic magmas at sulfide saturation and applications to magmatic sulfide deposit. *Miner. Depos.* **2005**, *40*, 218–230. https://doi.org/10.1007/s00126-005-0478-8
76. Hoatson Dean, M.; Keays Reid, R. Formation of platiniferous sulfide horizons by crystal fractionation and magma mixing in the Munni Munni layered intrusion, West Pilbara Block, Western Australia. *Econ. Geol.* **1989**, *84*, 1775–1804. https://doi.org/10.2113/gsecongeo.84.7.1775
77. Keays.; Reid R. The role of komatiitic and picritic magmatism and S-saturation in the formation of ore deposits. *Lithos* **1995**, *34*, 1–18. https://doi.org/10.1016/0024-4937(95)90003-9
78. Barnes, S.J.; Maier, W.D. Platinum-group element distributions in the Rustenberg Layered Suite of the Bushveld Complex, South Africa. In *The Geology, Geochemistry, Mineralogy and Mineral Beneficiation of Platinum-Group Elements*; Cabri, L.J., Ed.; Canadian Institute of Mining, Metallurgy and Petroleum: Montreal, QC, Canada, 2002; Special Volume 54.